Reduction kinetics of CoO-NiO/Al_2O_3 oxygen carrier for chemical-looping combustion

M. M. Hossain, H. I. de Lasa
CREC and Department of Chemical & Biochemical Engineering, The University of Western Ontario, London, ON, Canada N6A 5B9

Abstract

This communication reports the reduction mechanism and kinetics of CoO-NiO/Al_2O_3 oxygen carrier using methane as the reduction gas. Kinetics experiments are performed in a novel fluidized bed CREC riser simulator under turbulent fluidized bed reaction conditions. A shrinking-core model is used for the kinetic modeling assuming spherical grains of the oxygen carrier particles. The XRD analysis showed that in the bimetallic carrier, nickel is present mainly as NiO. Therefore, in particle conversion calculations NiO was considered as the only reducible oxide phase, under the selected reaction conditions. Mercury porosimetry revealed that the pore size of the carrier particle is slightly increased after reduction, which is an indication of a possible shrinking core model since the molar volume of Ni (6.6 cm^3/mol) is lower than that of NiO (7.54 cm^3/mol). The rate-controlling steps of the gas-solid reactions in CLC process is established by observing the reaction rates at different experimental conditions as well as using a number of the theoretical calculations i.e. Sherwood number, Weisz-Prater criterion for external and internal mass transfer limitations. It is shown that under the reaction conditions studied the chemical reaction between methane and the solid oxides controls the overall reduction rate. Temperature variation experiments show that the reduction reaction is a strong function of the thermal level, which further confirms the reaction controlling rate findings. The activation energy calculated from the shrinking-core model is 49 ± 10 kJ/mol with this being consistent with the literature values.

Keywords: CO_2 capture, CLC, reduction kinetics, unreacted shrinking core model

---

1. Introduction

In recent years, chemical-looping combustion (CLC) has been received growing interest as an energy efficient technology for CO_2 separation in gaseous-fueled combustion processes. Particularly, CLC technology is considered to be very promising to apply in the natural gas fired power generation systems. This non-conventional technique involves two interconnected fluidized beds, called fuel and air reactors (Fig. 1). A solid oxygen carrier circulates between the reactors to carryout the fuel combustion. In fuel reactor, the gaseous fuel is burned using the framework oxygen of the circulating oxygen carrier. The reduced oxygen carrier is then transported to the air reactor to reoxidize with air and finally recirculate back to the fuel reactor. A complete combustion of the fuel produces only CO_2 and water vapor and CO_2 can be recovered easily by condensing the water vapor without involving energy intensive special CO_2 separation processes. Finally, the pure CO_2 can be sequestrated or used for other applications. The outlet gas stream of the air reactor contains only nitrogen and unreacted oxygen, which is allowed to release to the atmosphere without risking any environmental damage. In addition to inherent CO_2 separation, the CLC also provides an extra opportunity to eradicate NO_x generation, which is equally important according to the environmental aspects. The CLC operates comparatively at low temperature and the fuel burns without any flame in absence of air, consequently no NO_x is formed during the combustion process.

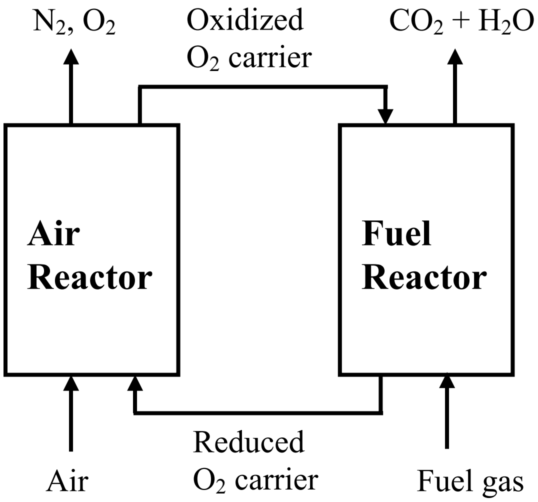

Figure 1: Conceptual diagram of a chemical-looping combustion processes.

Generally, the transition metal oxides such as nickel, copper, cobalt, iron and manganese have been considered to be suitable candidates for oxygen carriers. The above metal oxides are feasible for using as oxygen-carrying media due to their favorable thermodynamic properties. Apart from the thermodynamic feasibility, the oxygen carrier particles should have high reactivity in both the oxidation and reduction reactions, durability in repeated cycles, mechanical stability in fluidized bed reactor operation conditions and resistibility to agglomeration in the fluidized bed reactors (Mattisson et al, 2004; Adanez et *al.* 2004; Lyngfelt et al 2001; Cho et *al*. 2004). The other important considerations for a successful carrier are its economical feasibility and its environmental soundness. Most active metal oxides are not readily capable of providing all of the characteristics mentioned above. In order to increase reactivity, durability and fluidizability of the oxygen carrier particles are prepared by depositing the active metal oxide phase on an inert support, such as SiO_2, TiO_2, ZrO_2, Al_2O_3, and YSZ. In this respect, Hossain and de Lasa (2006) recently reviewed various oxygen carriers studied in literature. The iron and copper based materials are comparatively cheaper but the nickel-based carriers have several important advantages. For example, nickel can withstand higher temperatures, which is favorable to achieve higher performance in a gas turbine, and nickel is more efficient in carrying the oxygen as compared to iron or copper (Wolf et al, 2005). Another important feature of nickel is its negligible volatility until 1300 K (Villa et al, 2003). As a result, most of the previous studies concentrated on the nickel based oxygen carrier materials. However, to the date no oxygen carrier has claimed to fulfill all of the desirable characteristics for industrial scale application, which leaves the research area wide open to develop more suitable oxygen carrier material. In earlier articles, the present authors reported encouraging performance of a bimetallic Co-Ni/Al_2O_3 oxygen carrier in multiple reduction and oxidation cycles using methane and air for the respective reactions (Hossain et al. 2006a, 2006b). In such oxygen carriers a small amount of Co was added to alumina in order to promote the activity and stability of the oxygen carrier.

This communication, part of the development of bimetallic oxygen carrier for CLC power generation process, reports the reduction mechanism and kinetics of Co-Ni/Al_2O_3 oxygen carrier. The kinetics experiments are performed in a novel fluidized bed CREC riser simulator under turbulent fluidized bed reaction conditions. The shrinking-core model is used for the kinetics determination assuming spherical grains of the oxygen carrier particles. The rate-controlling steps of the gas-solid reactions in CLC process is defined by observing the reaction rates at different set of experimental conditions as well as applying the theoretical calculations i.e. Sherwood number, Weisz-Prater criterion for external and internal mass transfer limitations respectively.

2. Experimental

2.1. Preparation of oxygen carrier

The bimetallic oxygen carriers were prepared by the incipient wetness technique. The support α-Al_2O_3 (65% Al_2O_3, 34.8% H_2O, 0.15% Na_2O) was obtained from Stream Chemicals Inc. Three steps involved in oxygen carrier preparation: impregnation, reduction, and calcination. The detail procedure for oxygen carrier preparation can be found elsewhere (Hossain et al. 2006).

2.2. H_2 chemisorptions, X-Ray diffraction and pore measurements

The fresh calcined, fresh reduced and used oxygen carrier after multiple redox cycles were characterized using different physical and chemical techniques. The pulse chemisorptions experiments were carried out to determine active surface area, percent metal dispersion and active particle size of the carrier materials using a Micromeritics AutoChem II 2920 analyzer. During the pulse chemisorptions test, a stream of argon gas was flown through a bed of pre-reduced carrier at a rate of 50 mL/min. A series of hydrogen pulse (1.0 mL) were injected into the system at ambient temperature. A TCD detector analyzed the exit gas from the reactor. As hydrogen gas was adsorbed by the sample, peaks were created in the TCD reading of the outlet stream. The test was complete when two consecutive peaks had the same area.

The morphology of the carrier materials was studied using X-ray diffraction (XRD) analysis. The XRD experiments were performed in a Rigaku spectrometer at ambient temperature using Cu-Kα radiation (λ = 1.542 Å) at 10 kV and 50mA. The scan speed was 2 scan/min and 2θ value was ranges from 5 to 60 degree.

The porosity of Al_2O_3 support and the calcined and reduced Co-Ni/Al_2O_3 oxygen carrier particles were measured in a Micromeritics Mercury Pore Sizer 9010. The instrument determines the pore size of solid particles by assuming the cylindrical pore using the following equation.

$$d_{pore} = -\frac{4\sigma \cos\theta}{P_a} \qquad (1)$$

where, P_a applied pressure, σ is the surface tension and θ is the contact angle.

2.3. Kinetics experiments in CREC riser simulator

The experiments for kinetics investigation of the prepared oxygen carriers were carried out in a CREC Riser Simulator using methane as reducing gas. The CREC Riser Simulator is a bench scale mini-fluidized bed reactor, invented at CREC-UWO (de Lasa, 1992). This small size (capacity of 50 cm^3) reactor was designed for catalyst evaluation and kinetic studies under fluidized bed (riser/downer) reactor conditions. The CREC Riser Simulator consists of two sections: the upper and lower shells. These shells allow easy access to the reactor to load and unload the oxygen carrier. An impeller, located in the upper section, and a basket containing the solid oxygen carrier, located in the central section, are the main components of the reactor. Upon rotation of the impeller at high speed (up to 7000 rpm), gas is

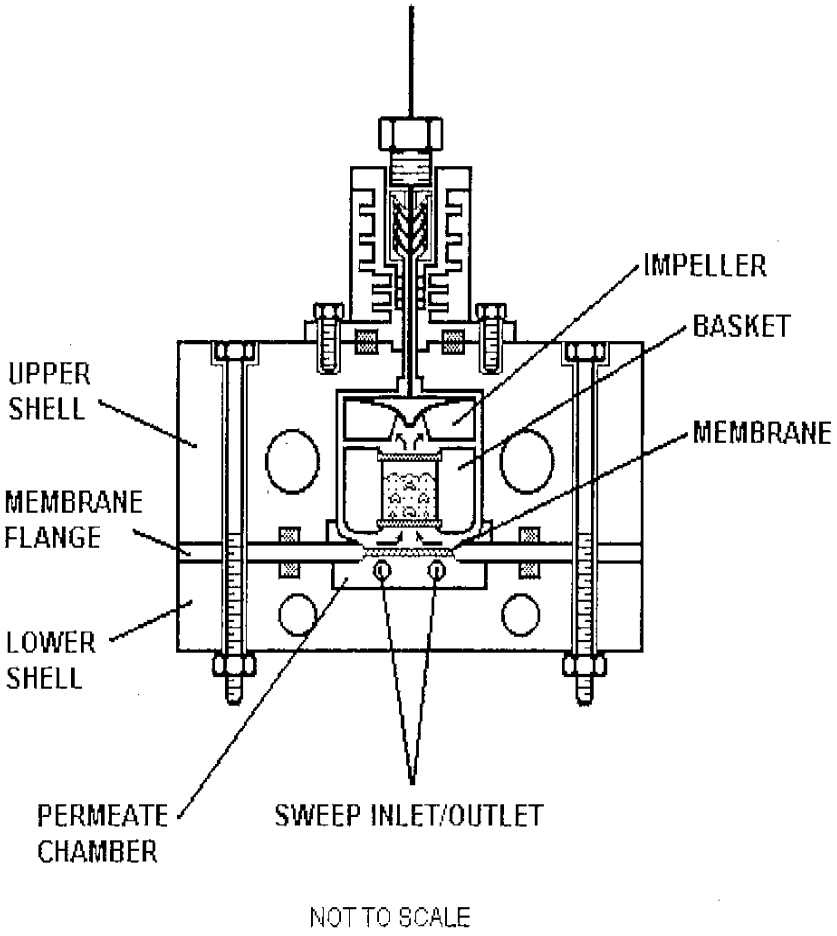

Figure 2: The CREC riser simulator.

forced both outward in the impeller section and downwards in the outer reactor annulus, causing the solids catalyst to become fully fluidized. A schematic diagram of the CREC-Riser Simulator is illustrated in Fig. 2.

For experiments, the solid oxygen carrier was first loaded into the reactor basket and then the reactor was reinstalled. The leak test was performed by monitoring the reactor pressure at closed conditions. The temperature program was run to heat up the system to desired temperature for the carrier reduction (combustion) reaction. An argon flow was maintained to ensure the system is free from air. Once the reactor reached thermal equilibrium, the argon flow was stopped and the vacuum box was brought into 3.0 psi using the vacuum pump. At this stage the impeller was turned on and the feed (CH_4) was injected into the reactor using a preloaded syringe. After the reaction proceeded for the specified time, the four-port valve was opened and the product was taken to the vacuum box. Finally, the product was analyzed using a gas chromatograph. Before the next cycle, the oxygen carrier was regenerated (oxidized) by flowing air at a specified temperature and time.

3. Results and discussions

3.1. Physicochemical characterization

In gas-solid reactions when supported metal oxides are involved as solid reactant the following complications might arise: (1) metal support interaction (2) preferred orientation of the active component (3) morphology and accessibility of the active species and (4) particle shape, size and pore size distribution. (Richardson et al, 2004). The physicochemical characterization of such kind of carrier material provides complete insight into the complex phenomenon and mechanisms. It also helps understanding the possible structural change of the carrier particles during the repeated oxidation-reduction cycles.

X-ray diffraction studies were carried out in order to identify the different phases of the nickel species present in the supported oxygen carrier. Fig. 3 shows the X-ray patterns of fresh calcined, reduced and used calcined oxygen carrier from a multiple CLC cycles. With both the fresh and used calcined samples, a strong signal for NiO at $2\theta = 43.519^{o}$ and relatively smaller peak for $NiCo_2O_4/NiAl_2O_4$ species at $2\theta = 37.519^{o}$ was observed. No Co_3O_4 peak was observed in the XRD patterns, which is understandably due to the low concentration of Co (0.5 %) in the carrier material. However, this small amount of Co shows significant effect in influencing the alumina support to minimize the $NiAl_2O_4$ formation. Generally, nickel has strong tendency to react with alumina to form difficult reducing $NiAl_2O_4$ but Co interacts more readily with alumina as compared to Ni, which allows nickel to form easily reducible NiO (Bolt et al. 1998). Even after multiple reduction/oxidation the crystalline structure of the oxygen carrier remained almost unchanged, which further indicates about stable behavior of the oxygen carrier and having minimum tendency of the nickel species to interact with the support. This result is consistent with the stable performance of similar oxygen carrier material during TPR/TPO experiments (Hossain et al, 2006). The crystal size of the metal particle of the reduced sample and metal dispersion was determined by H_2 chemisorption. The calculated size of the metal crystal and metal dispersion was about 80 nm and 1.8 % respectively. It is also apparent that the metal crystal size of the sample did not increase over repeated reduction/oxidation cycles, which is an indication of the minimum metal sintering during the cyclic reduction/oxidation processes. Relatively high and stable metallic surface area of the cobalt promoted carrier further supports the uniform and unchanged metal particle size (Hardiman et al. 2004a, 2004b, 2005, Takanabe et al, 2005).

The porosity of bare alumina support, fresh calcined, reduced and used samples were measured by mercury intrusion (Fig. 4). As it can be seen the pore size distribution of calcined alumina is bimodal. The first peak represents the pore sizes between 7.5 and 360 microns while the second peak consists of the pore size from 0.01 to 0.1 microns. After impregnation, the shape of the pore size distribution curves remains the same, except the first peak of the curve was shifted towards the lower range of pore size distribution. This decreased porosity is attributed to the clogging supports pores by metal species that makes them inaccessible for mercury intrusion. However, this is true only for the first peak of the pore size distribution curve because the second peak is remained unchanged after the metal loading, which suggests that the metal/metal oxide particles are larger than the largest pore of this peak. This observation is consistent with the particle size (80 nm) estimated by H_2 chemisorption because this size is small enough to get into the larger pores of the support as represented by the first peak and large enough to access the smaller pore of the second peak. Similar relation between the support pore size distribution and the metal particle size have been reported by Khodakov et al. (2002, 2003) in case of a silica supported Co catalysts.

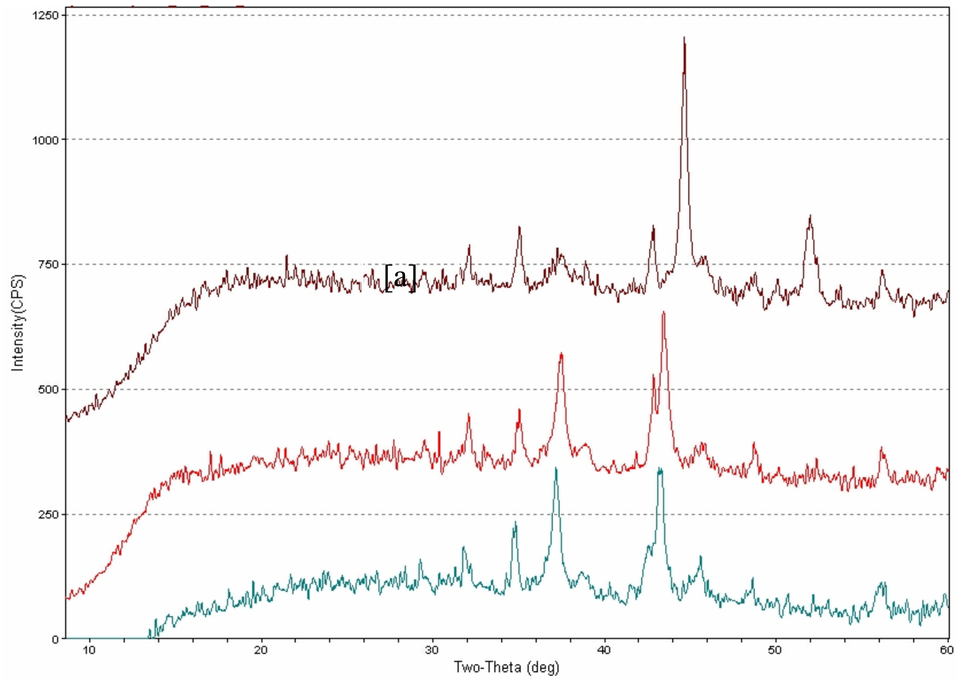

Figure 3: X-ray diffractograms of (a) freshly reduced (b) freshly calcined and (c) used (10 CLC cycles) Co-Ni/Al_2O_3 samples.

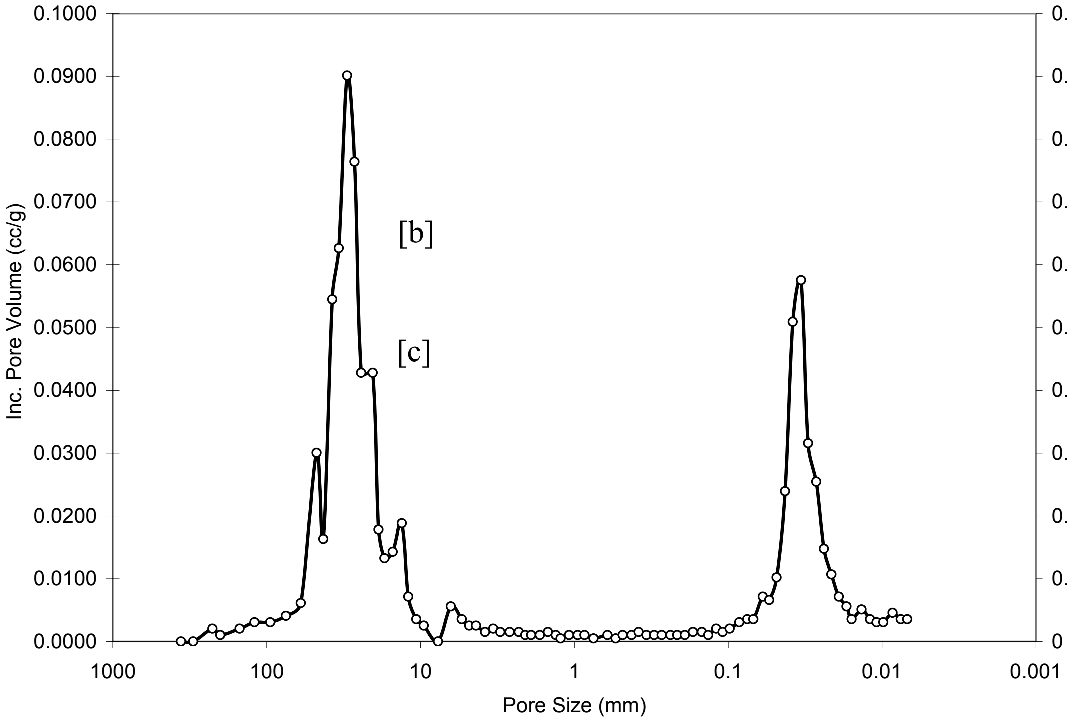

Figure 4a: Pore size distribution from Hg porosimetry for calcined Al_2O_3

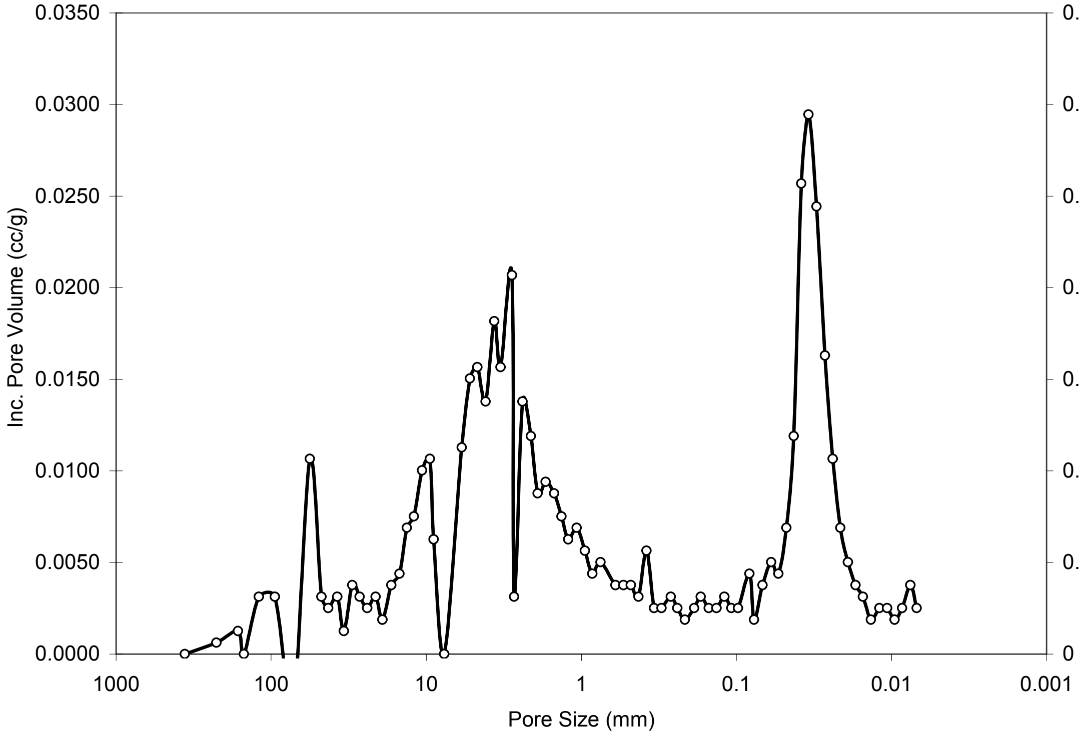

Figure 4b: Pore size distribution from Hg porosimetry for calcined Co-Ni/Al_2O_3.

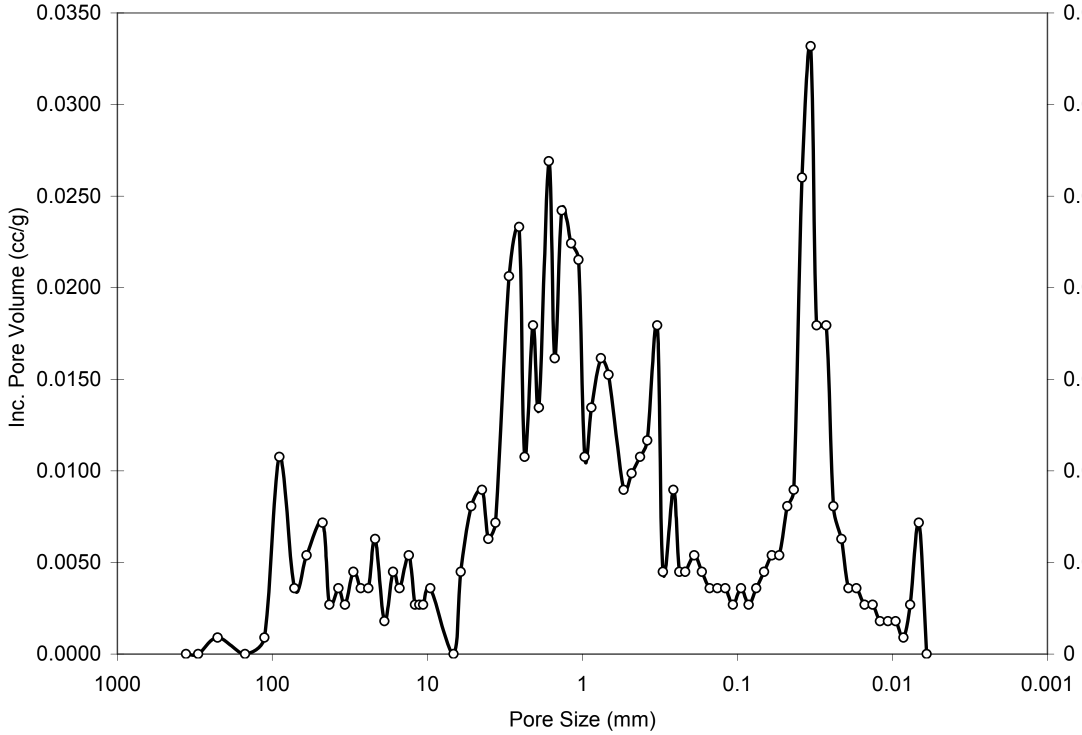

Figure 4c: Pore size distribution from Hg porosimetry for reduced Co-Ni/Al_2O_3.

3.2. Kinetics modeling

3.2.1. Phenomena involved

In CLC process both the fuel and air reactor involving gas-solid reactions. Before reacting with the solid reactant, the reactive gas molecules must be transported to the reaction site by (i) transferring from the bulk gas phase to the surface of the solid oxygen carrier and (ii) diffusion through the porous structure and through the blanket of the ash to the surface of the unreacted core of the solid material. Following the species transports steps; the reaction involves (iii) adsorption of the gas molecule on the active sites and (iv) reaction between adsorbed molecules and the solid phase. Finally, the gaseous product desorbs and transports to the bulk gas phase through steps (i) and (ii) but in the opposite direction. In chemical-looping combustion cycles each of the above steps has its own kinetics that can limit or influence to limit the overall rate of the reaction. In some situations some of the above steps do not exits. The resistances of the different steps also vary significantly. In such cases only the highest resistance has to be considered as rate-limiting step. For example, the reactions will be described as diffusion control regimes if the rate is determined by diffusion (external and/or internal) or chemical regime, when the rate is determined by the surfaces processes (adsorption/reaction/desorption). The kinetics rate-controlling steps of the gas-solid reactions in chemical-looping combustion process can be deduced by observing the reaction rate at different set of reaction conditions. The global reaction is considered to be the intrinsic if there are no transport limitations. Therefore, the first thing to examine is the possibility of transport limitation and if possible to eliminate otherwise has to account for. The external mass transfer limitation mainly depends on the particle size, the velocity between solid particle and fluid and the fluid properties. Therefore, the external transport limitation can be assessed both theoretically and experimentally. For experimental verification the reaction rate was measured at different speed of the impeller of the CREC riser simulator at constant temperature and contact time. High impeller speed reduces the thickness of the laminar boundary layer around the solid oxygen carrier, thus a lower mass transfer resistance can be expected. In the CREC riser simulator, the most of the fluidizable particles reaches turbulent fluidized bed conditions at a speed of 5700 rpm. For theoretical calculation the concentration gradient between the solid surface and the bulk fluid can be estimated from the Sherwood number with Froessling dimensionless correlation for a fluidized bed assuming spherical particles (Foglar, 1999).

$$Sh = 2 + 0.6 Sc^{1/3}\,\mathrm{Re}^{1/2} \tag{2}$$

$$k_c = \frac{Sh D_{AB}}{d_p} \tag{3}$$

$$-r'_{CH_4} = k_c\left(C_{CH_4} - C_{CH_4,S}\right) \tag{4}$$

Where, Sh, Sc and Re are Sharwood, Schmidt and Reynolds numbers, respectively. k_c is the external mass transfer co-efficient, D_{AB} molecular diffusivity, d_p is the particle diameter, $-r'_{CH_4}$ is the consumption rate of CH_4, C_{CH4} is the bulk concentration of methane, and $C_{CH4,S}$ is the surface concentration of methane. A higher Sherwood number indicates higher mass transfer rate and less gas film resistances. The value of Sharewood number varies in the range of 4-7 for the typical fluidized bed operation conditions. However, theoretically the lowest value is 2, occurs at stagnant fluid conditions around the solid particle. This lowest value corresponds to possible highest gas film resistances (minimum value of mass transfer coefficient). At minimum fluidized bed conditions the concentration gradient, calculated by using Eq. 4 is found negligible, therefore the reaction is free from external mass transport limitations. The possibility of the internal mass transfer effects has been assed theoretically by employing Weisz-Prater criterion (Foglar, 1999). The internal mass transfer may be negligible if the Weisz-Prater criterion is satisfied, namely:

$$C_{WP} = \frac{-r'_{CH_4}\rho_P R_P^2}{D_{eff} C_{CH_4}} << 1 \tag{5}$$

where, $-r'_{CH_4}$ is the consumption rate of CH_4 (mol/g solid. s) ρ_p is the particle density (g/cc), R_p is the particle radius (cm), D_{eff} is the effective diffusivity (cm^2/s) and C_{CH4} is the concentration of methane (mol/L). The Wiez-Prater parameter C_{WP}, was evaluated at worst possible reaction condition and the value obtained as 0.000175. This result confirmed that even under worst possible conditions, the internal mass transfer resistance was practically non-existent. Therefore, under the studied reaction conditions the chemical reaction between methane molecule and the solid oxides of the oxygen carrier control the reduction reaction.

3.2.2. The mathematical model

In general, the gas-solid reaction models are classified as (i) the homogeneous model, which consider the porous solid reactant as continuum, (ii) the grain model, which describe the solid reactant phase as a juxtaposition of dense objects and (iii) the pore model, which consider the porous solid as a collection of hollow objects (Patisson et al. 1998). Apart from the mass transfer limitations, considering the surface reaction, the models are only different in terms of structural description (grain or pores), which essentially leads to differences in calculating the surface area of the active sites. In fact, the models of the above classification are not totally independent and each of these models can possibly be derived from a more generalized mathematical form depending upon the appropriate structure of the solid material. Therefore, it was decided to derive a general texture model for methane combustion with Co-Ni/Al_2O_3 oxygen carrier and possibly cases were verified based on the physical characterization of Co-Ni/Al_2O_3 particles. The disappearance of the moles of solid reactant (oxygen) is given by

$$C_{NiO,0}\frac{dX_p}{dt} = br_m \tag{6}$$

where, $C_{NiO,0}$ is the initial molar concentration of NiO in the oxygen carrier, X_p is the particle conversion, b is the stoichiometirc coefficient of NiO and r_m is the rate of reaction per unit mass of the oxygen carrier, assuming the density of the carrier particles is not changed significantly during reduction. Since, the reaction is controlled by the chemical process, the reaction rate per unit mass in the balance equation can be directly related to the reaction per unit surface are of the solid particles, thus

$$r_m = a_0 S(X_p) r_s \tag{7}$$

where, a_0 is the initial specific surface area of oxygen carrier, r_s specific surface reaction rate and $S(X_p)$ reflects the change in the area of the reaction surface as a function of particle conversion. This function depends on the structure of the oxygen carrier particles. Combining last two equations yields

$$\frac{dX_p}{dt} = \frac{a_0 b}{C_{NiO,0}} S(X_p) r_s \tag{8}$$

In a gas-solid reaction the crystal size of solid reactant and the porosity of the support material often suggest important clues to the reaction kinetics. The porosity of the solid carrier will change if the molar volumes of the reactant and product solid materials are different

(Patisson and Ablitzer, 2002). As it has been already seen from the XRD and TPR data that in a Co-Ni/Al_2O_3 carrier the major species is NiO before reduction and Ni after reduction. According to equation 1,

$$CH_4 + 4NiO = CO_2 + 2H_2O \tag{10}$$

the stoichiometric ratio between the molar volume of NiO and Ni.

$$Z = \frac{4\upsilon_{Ni}}{4\upsilon_{NiO}} = \frac{4\times 6.59}{4\times 10.97} = 0.6 < 1 \tag{11}$$

Therefore, after reduction the porosity of the carrier material will be increased due to the shrinkage of the particle volume inside the pores. It has been already seen in the porosity analysis results that the porosity of the oxygen carrier sample was increased after reduction, which suggested a possible shrinking-core model might for the studied gas-solid reaction. Fig. 5 illustrates the schematics of the cyclic reduction and oxidation process described by spherical shrinking-core model. According to the shrinking-core spherical grain model the function $S(X_p)$ (in Eq. 8) can be expressed as

$$S(X_p) = (1 - X_p)^{2/3} \tag{12}$$

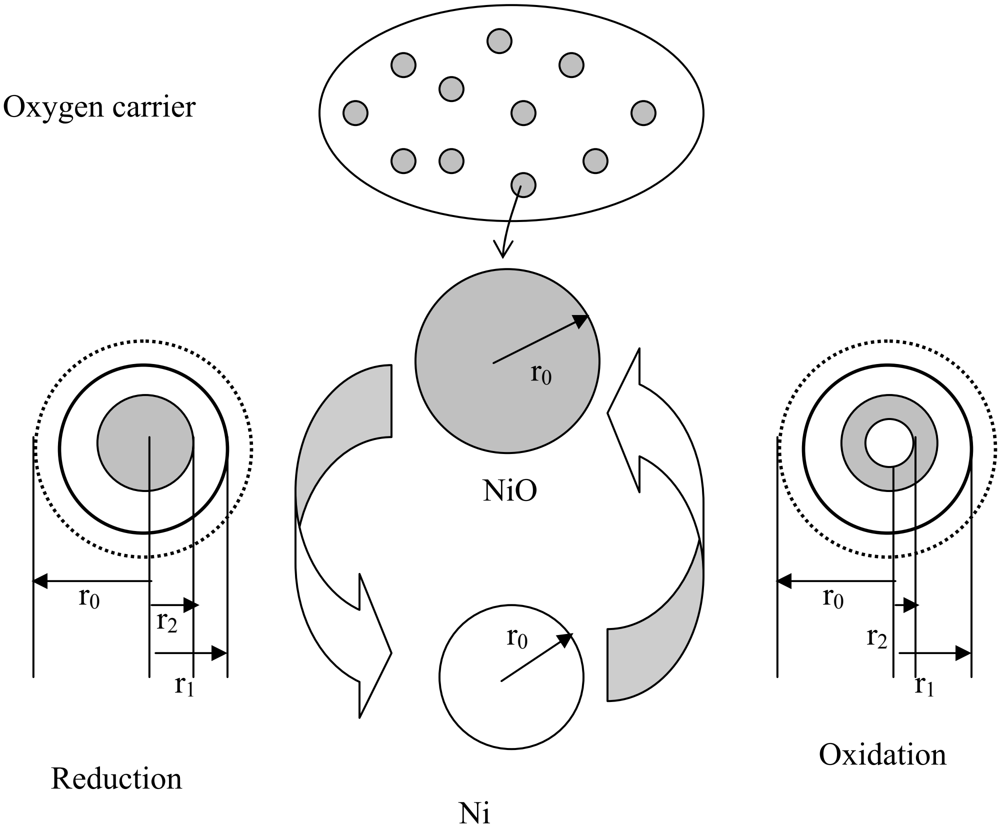

Figure 5: Scheme of the Shrinking-Core reaction model.

Finally, the surface reaction rate (r_s) can be derived assuming the reaction between the gas phase methane and solid NiO phase since both XRD and TPR result suggested negligible amount of aluminates was formed which was difficult to reduce in the studied reduction temperatures (550 to 650 ºC). Furthermore, earlier studies suggested that the alumina supported NiO reduction proceeds through adsorption of reducing gas (CH_4 in this case) on the NiO and/or Ni as they become available followed by rupture of Ni-O bonds to produce the metallic Ni, CO_2 and H_2O (Richardson et al. 2004; Bandrowski et al., 1962). In such models both adsorption and adsorption processes were considered faster than the surface reaction. Thus, considering a first order reaction with respect to methane the surface reaction rate can be formulated as.

$$r_s = k_s C_{CH_4} \tag{13}$$

or

$$r_s = k_s\left(1 - aX_p\right) \tag{14}$$

and

$$k_s = k_{s0} \exp\left[\frac{-E}{R}\left(\frac{1}{T} - \frac{1}{T_0}\right)\right] \tag{15}$$

the stoichiometric ratio between CH_4 and the oxygen carrier. Substituting Eq. 12, Eq. 14, and Eq. 15 into Eq. 8 yields,

$$\frac{dX_p}{dt} = k_0 \exp\left[\frac{-E}{R}\left(\frac{1}{T} - \frac{1}{T_0}\right)\right]\left(1 - X_p\right)^{2/3}\left(1 - aX_p\right) \tag{16}$$

where,

$$k_0 = \frac{a_0 b}{C_{NiO,0}} k_{s0} \tag{17}$$

3.2.3. Kinetics experiments and parameter estimation

The kinetics parameters of the prepared Co-Ni/Al_2O_3 oxygen carrier were determined by using CREC fluidized riser simulator data. As mentioned in the experimental section, this reactor can be operated in batch reactor mode under turbulent fluidized bed reactor conditions. Therefore, it allows generating conversion data for different reaction times, which is essential to estimate the kinetics parameters in the differential equation (Eq. 16) describing the reduction kinetics of the solid particles. Another important matter is the variation of the gas composition at various sections of the actual fluidized bed reactors. In fluidized bed CLC system the oxygen carrier is reduced by the gaseous fuel under different environments at different location of the fluidized bed reactors. At the bottom the of the fuel reactor the oxygen carrier particle will be in contact with only the pure fuel and along the length of the reactor the composition will be varied due to the formation of CO_2 and H_2O by combustion reaction. Therefore, the kinetics investigation experiments should incorporate those effects for their appropriate representation in the kinetics models and the estimated parameters. Fortunately, the turbulent mixing in the CREC fluidized bed riser simulator also simulates the effects of the formed products at different contact time (de Lasa, 1997). For further confirmation, several preliminary experiments were carried with different mixed feed (CH_4 and CO_2) compositions and found that the product CO_2 has no effect on the conversion of the oxygen carrier at studied reaction conditions. Gracia-Labiano et al. (2004) also reported the absence of product effects on the conversion of NiO and CuO based oxygen carriers. Consequently, the following experiments were carried out using pure CH_4 as feed. To determine the kinetics parameters the experiments were conducted in three different temperature levels (550 ºC, 600 ºC and 650 ºC) at constant reactor pressure. For each temperature level isothermal conversion data were collected for various reaction times.

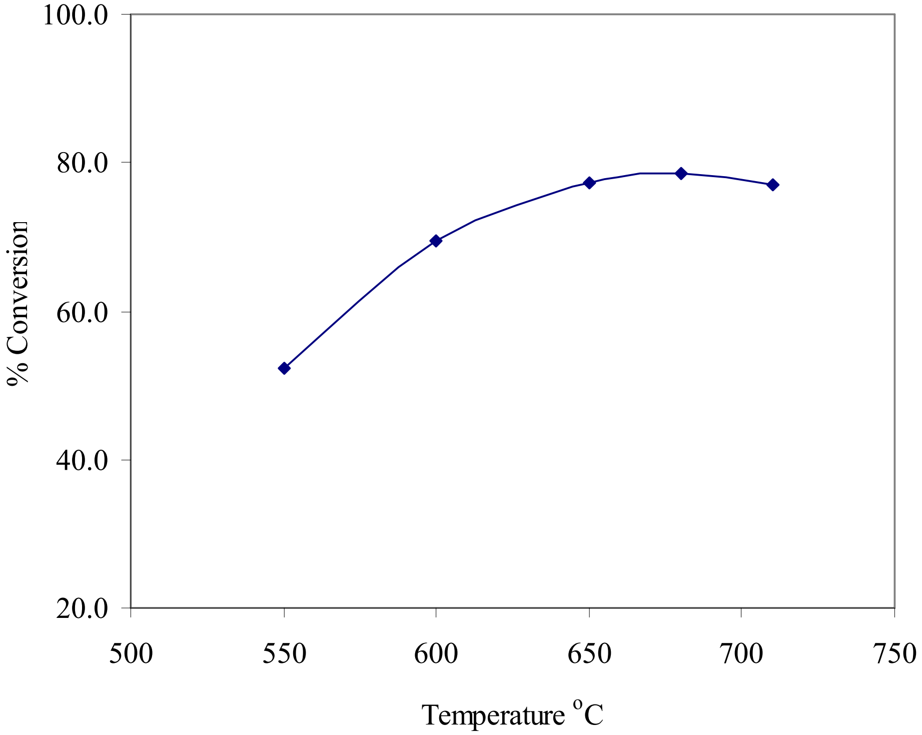

Figure 6: Effect of temperature on particle conversion using CH_4 as fuel in the CREC riser simulator.

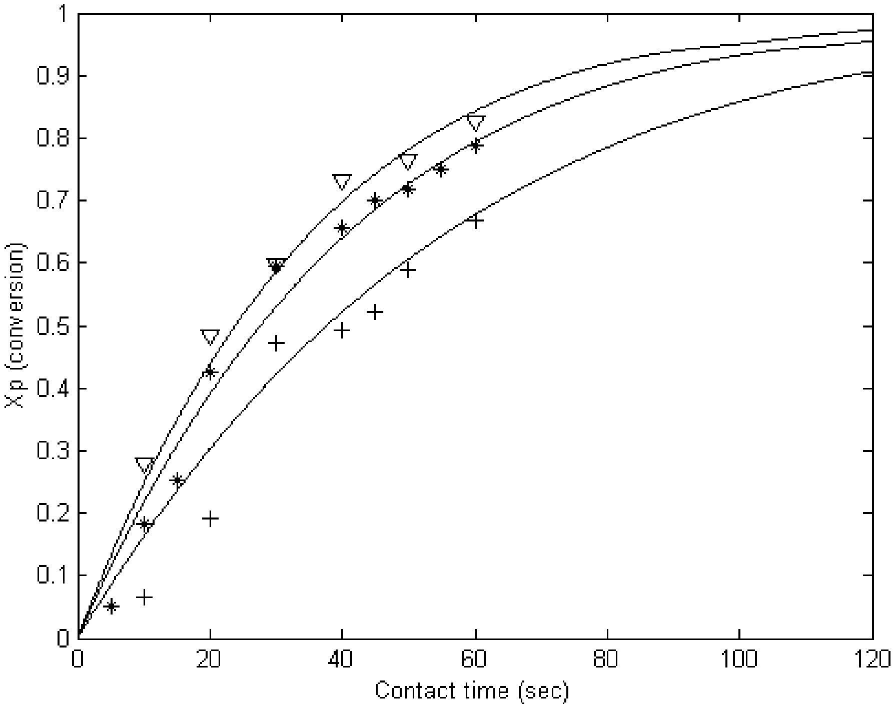

Figure 7: Comparison between experimental and model predicted conversion at different temperature.

The conversion data as function of temperature are shown in Fig. 6. It is clear that temperature has a strong influence on the reduction rate of the oxygen carrier particles, especially at lower temperature level. Isothermal reduction tests below 550 ºC showed that the reduction rate is very slow, and there appears to be an incubation period before reduction reaction started. The conversion of the solid particles was increased with increasing the temperature from 550 ºC to 600 ºC; approximately 80 % conversion was achieved in 60-sec reaction time. Further increasing the reaction temperature to 650 ºC also increased the conversion, however the increment was not as pronounced as between lower temperature levels. It was also observed that the incubation period was almost eliminated at higher temperature range.

In order to estimate the kinetics parameters in Eq. 16, simultaneous nonlinear regression analysis and solving the differential equation was performed using MATLAB program. In solving the differential equation the classical forth order Runge-Kutta method was applied. The estimated activation energy and pre-exponential factors with their 95 % confidence limits are 49 ± 10 (kJ/mole) and 8.4×10^{-11} respectively. The corresponding correlation coefficient for the estimated values is 0.97. Fig. 7 compares the experimental and model predicted particle conversion during the reduction reaction at different temperature levels. It is interesting to see that the shrinking-core model fits the high temperature data better than that of the low temperature data. The incubation period at low temperature is possible responsible for this discrepancy. Given the reasonable fitting of the experimental data, in can be argued that the shrinking-core model reasonable describe the reduction of CoO-NiO/Al_2O_3 oxygen carrier materials during the combustion cycle of the CLC processes. The estimated value of the activation energy of CoO-NiO/Al_2O_3 sample is similar to values of similar materials as summarized by Utigard et al (2005). The fairly high value of the activation energy for reduction of the supported carrier material further suggests that the reaction is chemical reaction controlled.

4. Conclusion

The reaction kinetics of the CoO-NiO/Al_2O_3 oxygen carrier material during the reduction cycle of the CLC process was investigated using methane as fuel in a novel fluidized bed CREC riser simulator. The kinetics model derived was based on the physicochemical characterization of the oxidized and reduced oxygen carrier and the experimental data from the CREC riser simulator. The porosity analysis experiments suggest that the pore size of the carrier particle was slightly increased after reduction, which is an indication of a possible shrinking core model since the molar volume of Ni (6.6 cm^3/mol) is lower than that of NiO (7.54 cm^3/mol). The calculated Sherwood number, Weisz-Prater criterion evaluated at extreme conditions shows that the reduction of CoO-NiO/Al2O3 with methane is free from both external and internal mass transfer limitations. The temperature variation experiments show as well, that the reduction reaction is a strong function of the temperature, which further confirms the reaction controlling rate formulations. In this regard, the shrinking-core model fits the higher temperature data better than that for the lower temperature data. The activation energies calculated from the shrinking-core model was 49 ± 10 kJ/mol, which this being consistent with reported literature values.

Acknowledgement

M.M.H. gratefully acknowledges the National Sciences and Engineering Research Council of Canada (NSERC) for Canada Graduate Scholarship for Doctoral study (CGS-D) and The University of Western Ontario for President's Scholarship for Graduate Study (PSGS).

References

Ananez, J., de Diego, L.F., Garcia-Labiano, F., Gayan, P., Abad, A. (2004), Selection of oxygen carriers for chemical-looping combustion, Energy & Fuels, 18, 371-377.

Bandrowski, J., Bickling, C.R., Yang, K.H., Hougen, O.A. (1962), Kinetics of the reduction of nickel oxide by hydrogen, Chemical Engineering Science 17, 379-390.

Bolt, P. H., Habraken, F. H. P. M., Geus, J. W. (1998), Formation of nickel, cobalt, copper, and iron aluminates form α- and γ-alumina-supported oxides: A comparative study, 135, 59-69.

Cho, P., Mattisson, Lyngfelt, A. (2004), Comparison of iron-, nickel-, copper-, and manganese-based oxygen carriers for chemical-looping combustion, Fuel, 83, 1245-1225.

de Lasa, H. I. (1992), Riser Simulator for Catalytic Cracking Studies, US Patent 5, 102, 628.

Foglar, H.S. (1999), Elements of Chemical Reaction Engineering, Prentice-Hall, Englewood Cliffs, NJ.

Garcia-Labiano, F., de Diago, L.F., Adanez, J., Abad, A., Gayan, P. (2005), Temperature variations in the oxygen carrier particles during their reduction and oxidation in a chemical-looping combustion system, Chemical Engineering Science 60, 851-862.

Hardiman, K. M., Cooper, C. G., Adesina, A. A. (2004), Multiple analysis of the role of preparation conditions on the intrinsic properties of Co-Ni/Al_2O_3 steam-reforming catalyst, Industrial and Engineering Chemistry Research, 43, 6006-6013.

Hardiman, K. M., Hsu, C. H., Ying, T. T., Adesina, A. A. (2005), The influence of impregnating pH on the postnatal and steam reforming characteristics of a Co-Ni/Al_2O_3 catalyst, Journal of Molecular Catalysis A: Chemical, 239, 41-48.

Hardiman, K. M., Ying, T. T., Adesina, A. A., Kennedy, E. M., Dlugogorski, B. Z. (2004), Performance of a Co-Ni catalyst for propane reforming under low steam-to-carbon ratios, Chemical Engineering Journal, 102, 119-130.

Hossain, M.M., de Lasa, H.I. (2006), Development of novel chemical-looping combustion (CLC) for inherent CO_2 separation – a review, International Journal of Chemical Reactor Engineering (accepted).

Hossain, M.M., Sedor K.E., de Lasa, H.I.(2006), Co-Ni/Al_2O_3 oxygen carrier for fluidized bed chemical-looping combustion: Desorption kinetics and metal support interaction, Chemical Engineering Science (ISCRE 19 – special issue).

Hossain, M.M., de Lasa, H.I. (2006), Reactivity and stability of Co-Ni/Al_2O_3 oxygen carrier in multicycle fluidized bed chemical-looping combustion (To be submitted to Chemical Engineering Science).

Khodakov, A.Y., Bechara, R., Griboval-Constant, A.(2003), Fischer-Tropsch synthesis over silica supported cobalt catalysts: mesoporous structure versus cobalt surface density, Applied Catalysis A: General 254, 273-288.

Khodakov, A.Y., Griboval-Constant, A., Bechara, R., Zholobenko, V.L. (2002), Pore size effects in Fischer Tropsch synthesis over cobalt-supported mesoporous silicas, Journal of Catalysis, 206, 230-241.

Lyngfelt, A., Leckner, B., Mattisson, T. (2001), A fluidized-bed combustion process with inherent CO_2 seperation; application of chemical-looping combustion, Chemical Engineering Science, 56, 3101-3113.

Mattisson, T., Johansson, M. Lyngfelt, A. (2004), Multicycle reduction and oxidation of different types of iron oxide particles-Application to chemical-looping combustion, Energy & Fuel, 18, 628-637.

Patisson, Ablitzer, D. (2002), Physicochemical and thermal modeling of the reaction between porous pellet and gas, Powder Technology 128, 300-305.

Patisson, F., Francois, M.G., Ablitzer, D. (1998), A non-isothermal, non-equimolar transient kinetics model for gas-solid reactions, Chemical Engineering Science 53, 697-708.

Richardson, J.T., Scates, R.M., Twigg, M.V. (2004), X-ray diffraction of hydrogen reduction of $NiO/\alpha\text{-}Al_2O_3$ steam reforming catalysts, Applied Catalysis A: General 267, 35-46.

Takanabe, K., Ngaoka, K., Nariai, K., Aika, K. (2005), Titani-supported cobalt and nickel bimetallic catalysts for carbon dioxide reforming of methane, Journal of Catalysis, 232, 268-275.

Utigard, T.A., Wu, M., Plascencia, G., Martin, T. (2005), Reduction kinetics of Goro nickel oxide using hydrogen, Chemical Engineering Science 60, 2061-2068.

Villa, R., Cristiani, C., Groppi, G., Lietti, L., Forzatti, P., Cornaro, U., Rossini, S. (2003), Ni based mixed oxide materials for CH_4 oxidation under redox cycle conditions, Journal of Molecular Catalysis A: Chemical 204-205, 637-646.

Wolf, J., Anheden, M., Yan, J. (2005), Comparison of nickel- and iron-based oxygen carriers in chemical looping combustion for CO_2 capture in power generation, Fuel, 84, 993-1006.